Thermopower and Nernst measurements in a half-filled lowest Landau level

Xiaoxue Liu,[1,*] Tingxin Li,[2] Po Zhang,[1] L. N. Pfeiffer,[3] K. W. West,[3] Chi Zhang,[1,4] and Rui-Rui Du[1,2,4,†]

[1]*International Center for Quantum Materials, School of Physics, Peking University, Beijing 100871, China*

[2]*Rice University, Houston, Texas 77251-1892, USA*

[3]*Princeton University, Princeton, New Jersey 08544, USA*

[4]*Collaborative Innovation Center of Quantum Matter, Beijing 100871, China*

(Received 13 January 2018; revised manuscript received 13 May 2018; published 28 June 2018)

Motivated by the recent proposal by Potter *et al.* [Phys. Rev. X **6**, 031026 (2016)] concerning possible thermoelectric signatures of Dirac composite fermions, we perform a systematic experimental study of thermoelectric transport of an ultrahigh-mobility GaAs/$Al_xGa_{1-x}As$ two-dimensional electron system at filling factor $\nu = 1/2$. We demonstrate that the thermopower S_{xx} and Nernst S_{xy} are symmetric and antisymmetric with respect to $B = 0$ T, respectively. The measured properties of thermopower S_{xx} at $\nu = 1/2$ are consistent with previous experimental results. The Nernst signals S_{xy} of $\nu = 1/2$, which have not been reported previously, are nonzero and show a power-law relation with temperature in the phonon-drag dominant region. In the electron-diffusion dominant region, the Nernst signals S_{xy} of $\nu = 1/2$ are found to be significantly smaller than the linear temperature dependent values predicted by Potter *et al.*, and decreasing with temperature faster than linear dependence.

DOI: 10.1103/PhysRevB.97.245425

I. INTRODUCTION

The composite fermions (CFs) paradigm has been remarkably successful in our understanding of the fractional quantum Hall effect (FQHE) [1–3]. Halperin, Lee, and Read (HLR) proposed the CFs as being one electron interacting with two Chern-Simons fluxes in a half-filled lowest Landau level (LL) [4]. At the mean field level, at $\nu = 1/2$, the average Chern-Simons gauge field precisely cancels the external magnetic field, so the effective magnetic field seen by CFs is zero and the electronic state of half filling is regarded as a compressible metallic state of CFs with a distinct Fermi surface. When filling factors deviate from $\nu = 1/2$, CFs execute the semiclassical cyclotron orbits under an effective magnetic field $\Delta B = B–B_{1/2}$, resembling cyclotron motion of electrons under low magnetic field. Results of major experimental studies concerning $\nu = 1/2$ states including surface acoustic wave [5,6], magnetic focusing [7], and geometric resonance [8] are remarkably consistent with HLR theory.

Son recently emphasized [9,10] that, contrary to the belief that the particle-hole symmetry (PHS) should be preserved for the spin-polarized lowest half-filled Landau level states in the limit of negligible Landau level mixing [11–16], PHS is not explicitly built in by HLR theory. Son proposed a particle-hole symmetric quasifermionic picture for $\nu = 1/2$ – massless Dirac composite fermions (DCFs), and the Dirac nature means that there exists a Berry phase of π around the Fermi surface of CFs [9,10]. On the other hand, it has been pointed out that the proposal of DCF is not entirely different from HLR theory, since it could evolve into the picture of HLR by introducing particle-hole symmetry broken mass [9,10]. The DCF framework has attracted much attention, largely because it may reveal deep connections between the fractional quantum Hall effect and other physical systems, such as time reversal symmetry protected topological insulators [17–24]. From the viewpoint of PHS, the work [9,10] has since stimulated several proposals [25–27] to experimentally examine the evidence for PHS, or lack of it, in a half-filled lowest Landau level.

Electrical transport has been a common and most important probe in studies concerning the $\nu = 1/2$ states [28–32]; however, the difference in transport data between HLR and DCF theory, as proposed in Ref. [9], is difficult to discern in realistic experiments. On the other hand, as recently proposed by Potter *et al.* [25], Nernst measurement is a direct and quantitative probe for the Berry phase. Note that the Nernst signal should probe the Berry phase around the CF Fermi surface, not necessarily the Dirac dispersions, so it should reveal general fermiology of composite fermions around $\nu = 1/2$.

We now briefly review thermoelectric transport of electrons in a temperature gradient and under a perpendicular magnetic field. Electrons will move from the hotter end to the colder end by thermal diffusion or momentum transfer with phonons (called phonon drag). Note that, among these two contributions, the electron diffusion is dominant at the low-temperature region, and the phonon drag plays a predominant role at increasing temperatures. A built-in electric field pointing to the cold end will be generated, so the electrical current can be written as $j = \hat{\sigma}(E) + \hat{\alpha}(-\nabla T)$, where $\hat{\sigma}$ and $\hat{\alpha}$ are electrical conductivity and thermal conductivity tensors, respectively. When $j = 0$, corresponding to the situation in which the diffusion current is equal to the drift current but with an opposite sign, the formula above could be written as $E = \hat{S}\nabla T$, where $\hat{S} = \hat{\alpha}/\hat{\sigma}$ or $\hat{S} = \hat{\alpha} \cdot \hat{\rho}$ is the Seebeck tensor. Here $\hat{\rho}$ is the electrical resistivity tensor, $\hat{\rho} = \hat{\sigma}^{-1}$. Thermopower

*lxxue@pku.edu.cn

†rrd@rice.edu

 ©2018 American Physical Society

S_{xx} refers to the diagonal part of $\hat{S}$ and Nernst-Ettingshausen S_{xy} corresponds to the off-diagonal part of $\hat{S}$, where $S_{xx} = \rho_{xx}\alpha_{xx} - \rho_{yx}\alpha_{yx}$ and $S_{xy} = \rho_{xy}\alpha_{xx} + \rho_{xx}\alpha_{xy}$.

According to Potter *et al.*, HLR and DCF can be distinguished by thermoelectric measurements [25]. Specifically, the Nernst coefficient S_{xy} in the diffusion-dominant region, where phonon drag is negligible, has a more direct and sensitive relationship with the Berry phase around the Fermi surface of CFs. S_{xy} is nonzero for the DCF theory with a PHS protected π Berry phase, and zero for PHS-broken HLR theory without the Berry phase [25]. However, a recent analysis [33] indicates that HLR theory has an emergent PHS and is equivalent to DCF theory in the limit of long wavelengths and low energies. When HLR theory is treated properly, Nernst coefficients of $\upsilon = 1/2$ for HLR theory should be nonzero as well [33]. Accordingly, the purpose of thermoelectric experiments should be to study the conditions under which PHS is preserved in realistic material systems, rather than to distinguish between the two theories.

In this paper, we systematically investigate the dc transport and thermoelectric properties of the $\upsilon = 1/2$ state in a high-mobility two -dimensional electron system hosted in $GaAs/Al_xGa_{1-x}As$ materials. In our thermoelectric transport measurements, thermopower S_{xx} and Nernst S_{xy} clearly exhibit, respectively, symmetric or antisymmetric signals with respect to $B = 0$ T, over the measured temperature (T) range. At the filling factor $\upsilon = 1/2$, where composite fermions form a compressible Fermi liquid in a zero effective magnetic field, thermopower S_{xx} shows a linear relation with T in the diffusive region, while it shows a power-law T dependence for the phonon-drag region. This is analogous to the thermopower S_{xx} of electrons in a zero magnetic field, and is consistent with previous experimental results [34–36]. As for the measured Nernst signals S_{xy} of $\upsilon = 1/2$, in the phonon-drag region, they exhibit an expected power-law relation with T. In the electron-diffusion dominated region, for the particle-hole symmetric $\upsilon = 1/2$ state, a Nernst signal S_{xy} with linear T dependence is predicted [25,33]. However, the Nernst signals of $\upsilon = 1/2$ in this regime are found by our experiment to be significantly smaller than the values with linear temperature dependence predicted by Potter *et al.* [25], and it decreases with temperature faster than linear dependence.

II. EXPERIMENTAL METHOD

A. Sample characterization

The data presented here are obtained from a high-mobility $GaAs/Al_{0.24}Ga_{0.76}As$ heterojunction wafer grown by molecular beam epitaxy. After a brief illumination from a red light-emitting diode, the density and mobility (measured at 60 mK) are 0.92×10^{11} cm^{-2} and 1.1×10^7 cm^2/V s, respectively. A 100-μm-wide Hall bar mesa was patterned on a piece of wafer (size of 10 mm $\times$ 1.7 mm $\times$ 0.5 mm) by photolithography and wet etching. Electrodes were defined by e-beam lithography, followed by Ni/GeAu evaporation and annealing process. A heater made of Ti/Au films was fabricated on one end of the sample, while the other end was indium soldered to a copper cold finger which serves as the thermal ground. A schematic of the device is shown in Fig. 1(a). The measurement was carried out in a dilution refrigerator equipped with an 8.5 T superconducting solenoid.

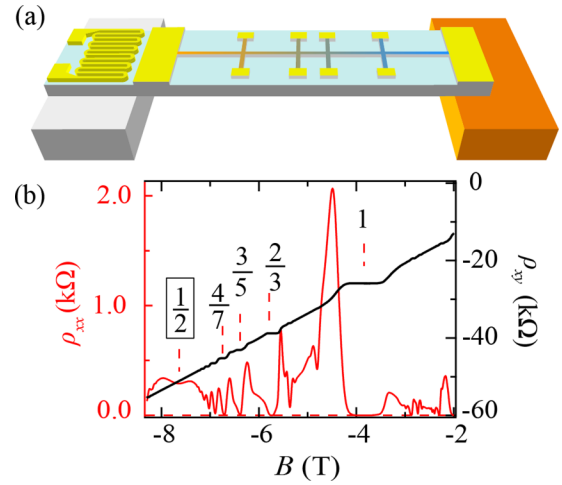

FIG. 1. (a) Sketch map of the device used in our thermoelectric transport measurement. (b) Longitudinal resistivity ρ_{xx} and Hall resistivity ρ_{xy} vs magnetic field at $T = 60$ mK.

To characterize the sample, we performed the electrical transport measurements using the standard lock-in technique with an excitation current of 10 nA at $f = 17$ Hz. The electrical transport results are shown in Fig. 1(b), which shows well-developed high-order FQHE states, attesting to the high mobility and the high degree of density homogeneity.

B. Measurement method

In thermoelectric transport experiments, thermometers are usually attached to the back of the sample, but this will induce a strain effect for high-mobility $GaAs/Al_xGa_{1-x}As$ heterostructure samples, or create a nonuniform temperature gradient. To determine temperature differences without these drawbacks, we adopted the method of integrating the thermal conductance along the sample [36], so before the thermoelectric measurement was carried out, we first measured the temperature dependence of the sample's thermal conductivity κ, which is dominated by phonon thermal transport.

The procedure for determining thermal conductivity κ of our sample is as follows. First, the temperature of the cold finger is maintained at T_i (which is read by a calibrated ruthenium oxide sensor), and the resistance minimum R_{xx} at $\upsilon = 4/3$ is measured. Note that R_{xx} at $\upsilon = 4/3$ has a strong temperature dependence over the measurement temperature range between 100 and 350 mK, so R_{xx} (4/3) as a function of T can be used as an effective thermometer. Next, R_{xx} (4/3) is measured at the temperature of cold finger $T_i + \Delta T$, where the temperature increment $\Delta T < 10\% T_i$. The above measurement is carried out without applying any power to the heater so that the temperature of the cold finger equals the temperature of 2DEG (two-dimensional electron gas). Subsequently, we hold the temperature of the cold finger at T_i again, and adjust the power $\dot{Q}$ applied to the heater until R_{xx} (4/3) becomes close to that at temperature $T_i + \Delta T$. The temperature gradient arising from the introduction of power $\dot{Q}$ is thus determined. According to

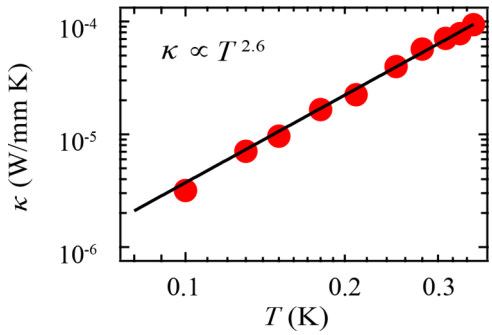

FIG. 2. The thermal conductivity κ shown as red circles as a function of temperature. The black line is the fit to the data; it exhibits a power-law relation of $T^{2.6}$.

$K = \dot{Q}/\Delta T$, we calculate the thermal conductance K, which is between the middle of two measurement contacts and the cold end. The thermal conductance K is further divided by the geometric factors of the sample, to obtain the thermal conductivity κ. By repeating the above procedure at different T_i, the temperature dependence of thermal conductivity κ can be systematically determined, which is shown in Fig. 2. As shown in Fig. 2, the thermal conductivity κ is found to follow a power law against T: i.e., $T^{2.6}$. The power exponent is reasonably close to that expected for phonon dominated heat transport.

To perform the thermoelectric measurement, a controllable temperature gradient ∇T was established along the Hall bar by applying a low frequency ($f = 7.3$ Hz) ac current to the heater. The thermal voltage ΔV between a pair of contacts along the gradient was measured by the lock-in technique at the frequency of $2f = 14.6$ Hz. The temperature value was obtained by integrating the thermal conductance K of the sample, combining the temperature of the cold finger and the applied power of the heater. The temperature or voltage gradient was further calculated according to the dimension of the Hall bar. When sweeping the perpendicular magnetic field, the thermopower S_{xx} and Nernst S_{xy} will then be determined by $S_{xx} = \nabla V_{xx}/\nabla T_x$ and $S_{xy} = \nabla V_{xy}/\nabla T_x$, respectively. Note here an "open circuit" condition is satisfied assuming that the lock-in amplifier has infinite input impedance.

III. RESULTS AND DISCUSSIONS

Figure 3(a) displays the thermopower S_{xx} as a function of positive magnetic field B at different temperatures. Meanwhile, Nernst S_{xy}'s varying with sweeping B at different temperatures are shown in Figs. 4(a) and 4(b). The thermopower S_{xx} and Nernst S_{xy} show, respectively, symmetric or antisymmetric patterns with respect to $B = 0$ T. Both thermopower S_{xx} and Nernst S_{xy} increase in magnitude with increasing temperature.

Comparing the thermopower S_{xx} in Fig. 3(a) and resistivity ρ_{xx} in Fig. 1(b), we observe that thermopower S_{xx} exhibits oscillations of integer quantum Hall effect (IQHE) and fractional quantum Hall effect (FQHE), very much like ρ_{xx}. This is consistent with previous studies [34–36]. The IQHE and FQHE oscillations of S_{xx} have been well explained by existing theories. In particular, the diffusion thermopower S^d_{xx} of 2DEG

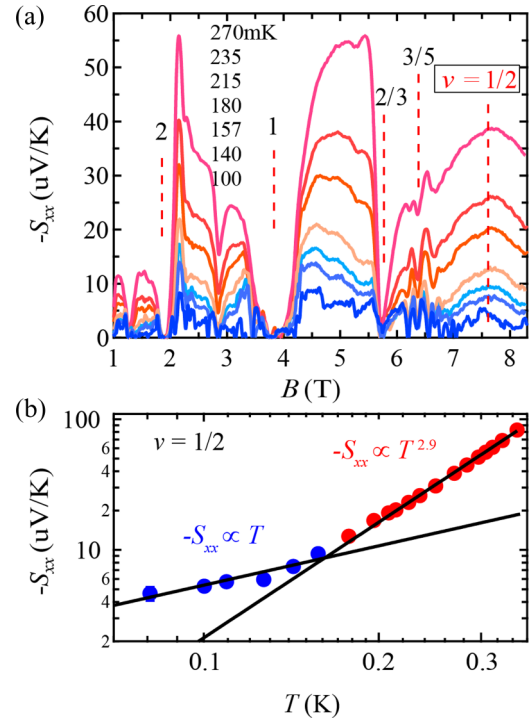

FIG. 3. (a) Longitudinal thermopower S_{xx} vs magnetic field B at different temperatures. Temperature labeled corresponds to traces from top to bottom. Several IQHE and FQHE states are marked. (b) The temperature dependence of S_{xx} at $\nu = 1/2$. Two black lines are the fit to the data in diffusion (blue circles) and phonon-drag (red circles) dominant regions, respectively. The S_{xx} of $\nu = 1/2$ shows a linear T dependence in the diffusion dominant region, while it shows a relation of $T^{2.9}$ for the phonon-drag dominant region. Note that the fitting to the linear regime is in the lower temperature region.

in the QHE regime is given by entropy per particle (quasiparticle) per charge [37–40]. The proportional expression between diffusion thermopower and entropy is in accordance with that of noninteracting electrons in a zero magnetic field predicted by the Mott formula [41]. Entropy will vanish when the chemical potential μ is in the gap of incompressible states, and attain maxima once μ is centered in the extended states of LLs. On the other hand, in the phonon-drag region, extended states of LLs with maximal density of states will be more likely to be scattered by phonons than localized states between LLs, leading to the oscillations of phonon-drag thermopower S^g_{xx} in B (similar to that of S^d_{xx}) [42,43]. However, although S^g_{xx} and S^d_{xx} have similar oscillations, their temperature dependences are entirely different: the diffusion S^d_{xx}, which is proportional to entropy, varies linearly with T, while the phonon-drag S^g_{xx} shows a power-law relation (with exponent ~3) as a function of T [39,41].

Figure 3(b) depicts the temperature dependence of thermopower S_{xx} of $\nu = 1/2$, where blue circles with error bars represent low-temperature thermopower S_{xx}, and red ones correspond to that at higher temperatures. Note that error bars represent the standard deviation from the average of S_{xx} (shown as circles). Quite clearly, at low temperatures $T < 160$ mK, electron diffusion is dominant, so the measured S_{xx} shows a linear relation as a function of T. With increasing temperature, phonon-drag thermopower contributes more to the signals,

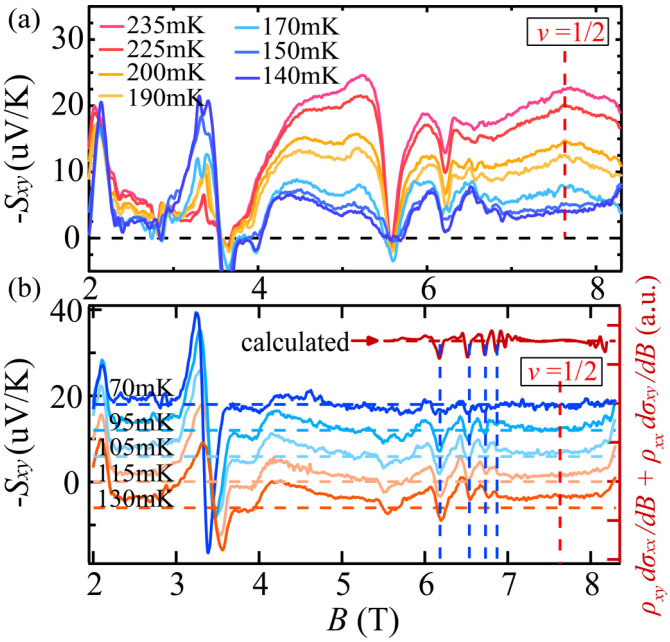

FIG. 4. (a) Nernst signals S_{xy} vs magnetic field B at different temperatures. Temperatures labeled correspond to traces from top to bottom. The $\nu = 1/2$ state is also labeled. (b) The topmost trace shows the calculated $\rho_{xx}d\sigma_{xy}/dB + \rho_{xy}d\sigma_{xx}/dB$ vs B in the FQHE regime around $\nu = 1/2$. The measured Nernst S_{xy} vs B below 130 mK are shifted vertically for clarity. Their corresponding base lines are shown as horizontal dashed lines and have the same color with measured traces. The $\nu = 1/2$ state and oscillations in the FQHE regime around $\nu = 1/2$ state are marked by vertical dashed lines.

leading to $S_{xx} \propto T^{2.9}$. The T dependence obtained from our measurements coincides well with previous results [34,35]. This comparison also serves as a test of our temperature calibration procedure. Notably, the T dependence of thermopower S_{xx} of the $\nu = 1/2$ compressible Fermi liquid is similar to those of noninteracting 2DEG at $B = 0$ T [39,41,44].

According to the prediction by Cooper *et al.* [39], diffusive thermopower S^d_{xx} at $\nu = 1/2$ can be regarded as entropy per quasiparticle per charge and can be written by the following expression, which is analogous to the Mott formula of 2DEG at $B = 0$ T,

$$S^d_{xx}\big|_{\nu=1/2} = -\frac{\pi k_B^2 m_{\rm CF}(1+p_{\rm CF})}{6\hbar^2 en}T. \qquad (1)$$

Here n is the density of 2DEG, $m_{\rm CF}$ is the effective mass of composite fermions determined by electron-electron interactions, and $p_{\rm CF}$ stands for the impurity scattering parameter of CFs. Due to the weak energy dependence of the impurity scattering rate of CFs [39], we take $p_{\rm CF} = 0$ here and apply Eq. (1) to our linear fit in Fig. 3(b). Note that the resulting slope (hence also the $m_{\rm CF}$ value) of the fit may be slightly dependent on the range of data points included. We find that the $m_{\rm CF}$ value spans roughly 0.92–0.97 m_e for including more data points towards the crossover point, where m_e is the mass of free electrons. Figure 3(b) shows the fit to all six points in the range, yielding $m_{\rm CF} \sim 0.97\, m_e$. Overall, the uncertainty of the mass value due to fitting is within 10%. This mass value is smaller than, but roughly agrees with, the previously reported $m_{\rm CF}(\nu = 1/2) \approx 1.5\, m_e\, (p_{\rm CF} = 0)$ obtained from thermopower measurements of 2DHS (two-dimensional hole system) [34]. It is larger than $m_{\rm CF}\,(\nu = 1/2) \approx 0.64\, m_e$ from magnetotransport measurement of 2DES around $\nu = 1/2$ [28]. Note that to facilitate the comparison we scale the $m_{\rm CF}\,(\nu = 1/2)$ values to the same magnetic field $B = 7.6$ T by $m_{\rm CF} \propto B^{1/2}$.

We now turn to the Nernst measurement results of $\nu = 1/2$ shown in Figs. 4(a) and 4(b). In realistic samples, the S_{xx} and S_{xy} components could couple to each other. Considering that Nernst S_{xy} is antisymmetric while the thermopower component S_{xx} mixed into S_{xy} is symmetric with respect to $B = 0$ T, by taking the sum and difference of the raw Nernst S_{xy} data under positive and negative magnetic field, we derive the "decoupled" Nernst S_{xy}, which is shown in Figs. 4(a) and 4(b). As shown in Fig. 4(a), for high-temperature region $T > 140$ mK, the Nernst signals in the vicinity of the $\nu = 1/2$ state increase rapidly with increasing T. As for the Nernst signals S_{xy} below 130 mK shown in Fig. 4(b), the measured traces at different temperatures are shifted vertically for clarity.

Theoretically, in the diffusion dominant regime, the semiclassical longitudinal and transverse thermopower of 2DEG under a low perpendicular magnetic field satisfy the generalized Mott formula,

$$S^d_{ij}(\varepsilon_F, T, B) = -\frac{\pi^2 k_B^2}{3e}\rho_{ik}\left[\frac{d\sigma}{d\varepsilon}\right]_{kj}\Bigg|_{\varepsilon=\varepsilon_F} T, \qquad (2)$$

where ε_F is the Fermi energy of electrons; ρ, σ are the electrical resistivity and conductivity tensors, respectively [37–39,45]. Moreover, Ref. [46] showed that Eq. (2) should be valid for weakly disordered noninteracting 2DEG in the QHE regime. In the QHE regime with high magnetic field, since $\rho_{xx} \ll \rho_{xy}$ and $\alpha_{xx} \ll \alpha_{xy}$, we obtain $S^d_{xx} \approx -\rho_{xy}\alpha_{xy}$ or $S^d_{xx} \propto \rho_{xy}\frac{d\sigma_{xy}}{dB}$. Therefore, S^d_{xx} will oscillate similarly to resistivity ρ_{xx} as a function of magnetic field B. As for the diffusion Nernst S^d_{xy}, theories predict that $S^d_{xy} \propto \rho_{xx}d\sigma_{xy}/dB + \rho_{xy}d\sigma_{xx}/dB$ [37,38,42]. Namely, when sweeping magnetic field in the QHE regime, a typical S^d_{xy} trace is expected to exhibit first a positive peak, then zero at the position of the maxima of ρ_{xx} or σ_{xx}, and finally a negative peak. In our experiments, as shown in Fig. 4(b), such feature of S^d_{xy} can be clearly observed in the vicinity of the IQH state $\nu = 1$ ($B \sim 3.5$ T).

Since the FQHE states around $\nu = 1/2$ can be viewed as the IQHE states of composite fermions, we apply Eq. (2) for analyzing thermoelectric transport in the FQHE regime around $\nu = 1/2$. We calculated $\rho_{xx}d\sigma_{xy}/dB + \rho_{xy}d\sigma_{xx}/dB$ by using the longitudinal resistivity ρ_{xx} and Hall resistivity ρ_{xy} of $T = 60$ mK; the calculated trace is shown in the top of Fig. 4(b). Remarkably, calculated electron-diffusion Nernst signals S^d_{xy} exhibit a series of oscillations in the FQHE regime around $\nu = 1/2$, and the period and dip positions of these oscillations (marked with blue vertical dashed lines in the figure) coincide well with our measured data. As shown in Fig. 4(b), these oscillations become more pronounced with the increasing of temperature, qualitatively consistent with the proportional relation between S^d_{xy} and temperature. We found a reasonable agreement between our experimental results and theoretical predictions, confirming that the measured Nernst

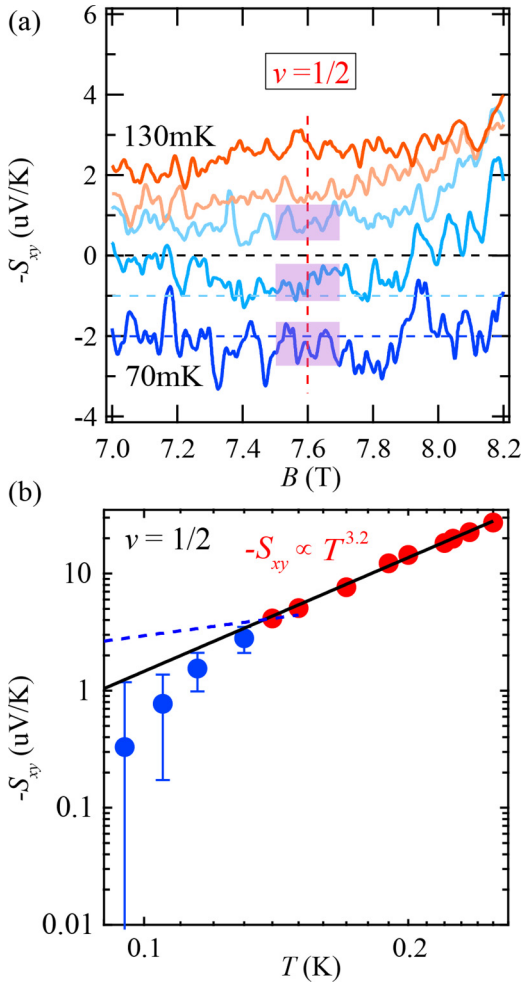

FIG. 5. (a) This shows a detail of Fig. 4(b), which is in the vicinity of $\nu = 1/2$. The $\nu = 1/2$ state is labeled. Only the two lowest temperature traces are shifted vertically. Their corresponding base lines are shown as horizontal dashed lines and have the same color with measured traces. Around $\nu = 1/2$, the traces of the three lowest temperatures are covered by a transparent rectangle. The rectangular width describes the maximum amplitude of signal fluctuations around $\nu = 1/2$ (between 7.5 and 7.7 T). (b) The temperature dependence of Nernst S_{xy} at $\nu = 1/2$. The data below 130 mK are shown as blue circles with error bars. The error bar here marks the uncertainty range described by the rectangular width shown in Fig. 5(a). The blue dashed line shows the predicted linear temperature dependent diffusion Nernst signals. The black line is the fit to data above 140 mK shown as red circles, which shows a power-law relation of $T^{3.2}$ with T.

signals at low temperatures (<130 mK) are indeed electron-diffusion dominant.

We now quantitatively analyze the data in the vicinity of $\nu = 1/2$. The S_{xy} vs B traces at the five lowest temperatures in the field range between 7 and 8.2 T are plotted in Fig. 5(a); only the two lowest temperature traces are shifted vertically. We note that here the measured Nernst signals S^d_{xy} at $\nu = 1/2$ drops precipitously towards low T. Around 100 mK the Nernst signals are of the same orders of magnitude as the background fluctuations (the amplitude of background voltage fluctuations is within ±5 nV).

We plot the Nernst signals of $\nu = 1/2$ against T in Fig. 5(b). The higher-T data (red solid circles) show a power-law relation $T^{3.2}$ with T down to a temperature $T \sim 140$ mK. At lower T (in the electron-diffusion regime), the predicted Nernst signals should cross over to a T-linear relation, as sketched by a dashed line in Fig. 5(b). Indeed the data (blue solid circles) begin to deviate from the $T^{3.2}$ fitting line at $T = 130$ mK. However, remarkably, the data eventually become significantly smaller than the predicted linear values (the blue dashed line), or for that matter even smaller than the values extrapolated from $T^{3.2}$.

At this point we do not have a concrete explanation for the observation of S^d_{xy} in the electron-diffusion regime. A nearly vanishing S^d_{xy} could indicate that the PHS is broken for the $\nu = 1/2$ state in our 2DEG system. A possible mechanism for broken PHS is inter-Landau-level mixing. Due to Coulomb interactions in the 2DEG system, inter-Landau -level mixing should exist in a finite magnetic field. For our low-density 2DEG sample, the $\nu = 1/2$ state is at $B = 7.6$ T, which corresponds to a substantial level of Landau level mixing. On the other hand, in the GaAs/AlGaAs 2DEG systems, the phonon drag to diffusive crossover occurs at a very low temperature (below 140 mK), where the electron-diffusion dominated Nernst signals are rather small, with their magnitudes comparable to the measurement systematic errors in our experiments.

IV. CONCLUSIONS

In summary, we have measured the longitudinal thermopower S_{xx} and transverse Nernst S_{xy} of compressible Fermi liquid states at filling factors $\nu = 1/2$ in a high-mobility GaAs/$Al_xGa_{1-x}As$ two-dimensional electron system. In the experimental temperature range, the thermopower S_{xx} and Nernst S_{xy} as a function of B show, respectively, the expected even or odd symmetry with respect to $B = 0$ T. Thermopower S_{xx} of $\nu = 1/2$ present a power-law relation with T in the phonon-drag dominant region, and a linear dependence on T in the diffusion dominant region, which is consistent with previous studies [34–36]. Furthermore, given the linear T fit of the diffusion thermopower and the generalized Mott formula [41], we determine the effective mass of composite fermions of $\nu = 1/2$ to be $0.97\,m_e$ for $\nu = 1/2$ at $B = 7.6$ T, where m_e is the mass of free electrons.

As for the Nernst signals S_{xy} of $\nu = 1/2$, in the phonon-drag dominant region, the Nernst signals S_{xy} are nonzero and have a power-law dependence on T. In the electron-diffusion dominant region, the S_{xy} show a series of oscillations in the FQHE regime around $\nu = 1/2$, which is consistent with the calculated results based on the generalized Mott formula. However, the measured diffusive Nernst signal of $\nu = 1/2$ is significantly smaller than the T-linear values predicted by relevant theory [25], and decrease with temperature faster than the linear dependence.

In this experiment the $\nu = 1/2$ state was set at a modestly high magnetic field $B = 7.6$ T, so the Landau level mixing is not negligible. The influence of Landau level mixing to broken PHS is an interesting theoretical issue which should be further addressed. We believe that the present study can provide a useful guide for more refined experiments. To increase the electron-diffusion Nernst signals, the S^d_{xy} of $\nu = 1/2$ may be measured in Si/SiGe heterostructures. Unlike that in the

piezoelectric GaAs/AlGaAs systems, the phonon drag in the Si/SiGe heterostructures is significantly suppressed below 1 K [47–49]. As a result, the S^d_{xy} of $\nu = 1/2$ could be obtained at higher temperatures with correspondingly larger diffusion Nernst signals.

ACKNOWLEDGMENTS

We acknowledge valuable discussions with A. H. MacDonald, J. K. Jain, and B. I. Halperin. We thank Changli Yang and Jian Mi for technical discussions. The work at Peking University was funded by National Basic Research Program of China (Grant No. 2014CB920901). The work at Rice was funded by NSF Grant No. DMR-1508644 and Welch Foundation Grant No. C-1682. The work at Princeton University was funded by the Gordon and Betty Moore Foundation through the EPiQS initiative Grant No. GBMF4420, by the National Science Foundation MRSEC Grant No. DMR- 1420541, and by the Keck Foundation.

[1] D. C. Tsui, H. L. Stormer, and A. C. Gossard, Two-Dimensional Magnetotransport in the Extreme Quantum Limit, Phys. Rev. Lett. **48**, 1559 (1982).

[2] R. B. Laughlin, Anomalous Quantum Hall Effect: An Incompressible Quantum Fluid with Fractionally Charged Excitations, Phys. Rev. Lett. **50**, 1395 (1983).

[3] J. K. Jain, Composite-Fermion Approach for the Fractional Quantum Hall Effect, Phys. Rev. Lett. **63**, 199 (1989).

[4] B. I. Halperin, P. A. Lee, and N. Read, Theory of the half-filled Landau level, Phys. Rev. B **47**, 7312 (1993).

[5] R. L. Willett, R. R. Ruel, K. W. West, and L. N. Pfeiffer, Experimental Demonstration of a Fermi Surface at One-Half Filling of the Lowest Landau Level, Phys. Rev. Lett. **71**, 3846 (1993).

[6] R. L. Willett, M. A. Paalanen, R. R. Ruel, K. W. West, L. N. Pfeiffer, and D. J. Bishop, Anomalous Sound Propagation at $\nu = 1/2$ in a 2D Electron Gas: Observation of a Spontaneously Broken Translational Symmetry? Phys. Rev. Lett. **65**, 112 (1990).

[7] V. J. Goldman, B. Su, and J. K. Jain, Detection of Composite Fermions by Magnetic Focusing, Phys. Rev. Lett. **72**, 2065 (1994).

[8] W. Kang, H. L. Stormer, L. N. Pfeiffer, K. W. Baldwin, and K. W. West, How Real Are Composite Fermions? Phys. Rev. Lett. **71**, 3850 (1993).

[9] D. T. Son, Is the Composite Fermion a Dirac Particle? Phys. Rev. X **5**, 031027 (2015).

[10] D. T. Son, The Dirac composite fermion of the fractional quantum Hall effect, Prog. Theor. Exp. Phys. **2016**, 12C103 (2016).

[11] S. M. Girvin, Particle-hole symmetry in the anomalous quantum Hall effect, Phys. Rev. B **29**, 6012 (1984).

[12] S. A. Kivelson, D.-H. Lee, Y. Krotov, and J. Gan, Composite-fermion Hall conductance at $\nu = 1/2$, Phys. Rev. B **55**, 15552 (1997).

[13] D.-H. Lee, Neutral Fermions at Filling Factor $\nu = 1/2$, Phys. Rev. Lett. **80**, 4745 (1998).

[14] E. H. Rezayi and F. D. M. Haldane, Incompressible Paired Hall State, Stripe Order, and the Composite Fermion Liquid Phase in Half-Filled Landau Levels, Phys. Rev. Lett. **84**, 4685 (2000).

[15] D. Kamburov, Y. Liu, M. A. Mueed, M. Shayegan, L. N. Pfeiffer, K. W. West, and K. W. Baldwin, What Determines the Fermi Wave Vector of Composite Fermions? Phys. Rev. Lett. **113**, 196801 (2014).

[16] M. Barkeshli, M. Mulligan, and M. P. A. Fisher, Particle-hole symmetry and the composite Fermi liquid, Phys. Rev. B **92**, 165125 (2015).

[17] D. F. Mross, A. Essin, and J. Alicea, Composite Dirac Liquids: Parent States for Symmetric Surface Topological Order, Phys. Rev. X **5**, 011011 (2015).

[18] C. Wang and T. Senthil, Dual Dirac Liquid on the Surface of the Electron Topological Insulator, Phys. Rev. X **5**, 041031 (2015).

[19] A. Karch and D. Tong, Particle-Vortex Duality from 3D Bosonization, Phys. Rev. X **6**, 031043 (2016).

[20] D. F. Mross, J. Alicea, and O. I. Motrunich, Explicit Derivation of Duality between a Free Dirac Cone and Quantum Electrodynamics in (2+1) Dimensions, Phys. Rev. Lett **117**, 016802 (2016).

[21] C. Wang and T. Senthil, Half-filled Landau level, topological insulator surfaces, and three-dimensional quantum spin liquids, Phys. Rev. B **93**, 085110 (2016).

[22] M. A. Metlitski and A. Vishwanath, Particle-vortex duality of 2D Dirac fermion from electric-magnetic duality of 3D topological insulators, Phys. Rev. B **93**, 245151 (2016).

[23] S. D. Geraedts, M. P. Zaletel, R. S. K. Mong, M. A. Metlitski, A. Vishwanath, and O. I. Motrunich, The half-filled Landau level: The case for Dirac composite fermions, Science **352**, 197 (2016).

[24] M. Mulligan, S. Raghu, and M. P. A. Fisher, Emergent particle-hole symmetry in the half-filled Landau level, Phys. Rev. B **94**, 075101 (2016).

[25] A. C. Potter, M. Serbyn, and A. Vishwanath, Thermoelectric Transport Signatures of Dirac Composite Fermions in the Half-Filled Landau Level, Phys. Rev. X **6**, 031026 (2016).

[26] A. K. C. Cheung, S. Raghu, and M. Mulligan, Weiss oscillations and particle-hole symmetry at the half-filled Landau level, Phys. Rev. B **95**, 235424 (2017).

[27] M. Levin and D. T. Son, Particle-hole symmetry and electromagnetic response of a half-filled Landau level, Phys. Rev. B **95**, 125120 (2017).

[28] R. R. Du, H. L. Stormer, D. C. Tsui, L. N. Pfeiffer, and K. W. West, Shubnikov–de Haas oscillations around $\nu = 1/2$ Landau Level Filling Factor, Solid State Commun. **90**, 71 (1994); R. R. Du, H. L. Stormer, D. C. Tsui, A. S. Yeh, L. N. Pfeiffer, and K. W. West, Drastic Enhancement of Composite Fermion Mass near Landau Level Filling $\nu = 1/2$, Phys. Rev. Lett **73**, 3274 (1994).

[29] R. R. Du, H. L. Stormer, D. C. Tsui, L. N. Pfeiffer, and K. W. West, Experimental Evidence for New Particles in the Fractional Quantum Hall Effect, Phys. Rev. Lett. **70**, 2944 (1993).

[30] L. P. Rokhinson, B. Su, and V. J. Goldman, Logarithmic temperature dependence of conductivity at half-integer filling factors: Evidence for interaction between composite fermions, Phys. Rev. B **52**, R11588 (1995).

[31] L. W. Wong, H. W. Jiang, and W. J. Schaff, Universality and phase diagram around half-filled Landau levels, Phys. Rev. B **54**, R17323 (1996).

[32] J. Zhang, R. R. Du, J. A. Simmons, and J. L. Reno, Resistance minimum observed at Landau level filling factor $\nu = 1/2$ in ultrahigh magnetic fields, Phys. Rev. B **81**, 041308 (2010).

[33] C. Wang, N. R. Cooper, B. I. Halperin, and A. Stern, Particle-Hole Symmetry in the Fermion-Chern-Simons and Dirac Descriptions of a Half-Filled Landau Level, Phys. Rev. X **7**, 031029 (2017).

[34] X. Ying, V. Bayot, M. B. Santos, and M. Shayegan, Observation of composite-fermion thermopower at half-filled Landau levels, Phys. Rev. B **50**, 4969 (1994).

[35] V. Bayot, E. Grivei, H. C. Manoharan, X. Ying, and M. Shayegan, Thermopower of composite fermions, Phys. Rev. B **52**, R8621 (1995).

[36] W. E. Chickering, J. P. Eisenstein, L. N. Pfeiffer, and K. W. West, Thermopower of two-dimensional electrons at filling factors $\nu = 3/2$ and $5/2$, Phys. Rev. B **81**, 245319 (2010); Thermoelectric response of fractional quantized Hall and reentrant insulating states in the $N = 1$ Landau level, *ibid.* **87**, 075302 (2013).

[37] M. Jonson and S. M. Girvin, Thermoelectric effect in a weakly disordered inversion layer subject to a quantizing magnetic field, Phys. Rev. B **29**, 1939 (1984).

[38] H. Oji, Thermopower and thermal conductivity in two-dimensional systems in a quantizing magnetic field, Phys. Rev. B **29**, 3148 (1984).

[39] N. R. Cooper, B. I. Halperin, and I. M. Ruzin, Thermoelectric response of an interacting two-dimensional electron gas in a quantizing magnetic field, Phys. Rev. B **55**, 2344 (1997).

[40] K. Yang, and B. I. Halperin, Thermopower as a possible probe of non-Abelian quasiparticle statistics in fractional quantum Hall liquids, Phys. Rev. B **79**, 115317 (2009).

[41] M. Cutler and N. F. Mott, Observation of Anderson localization in an electron gas, Phys. Rev. **181**, 1336 (1968).

[42] R. Fletcher, J. C. Maan, K. Ploog, and G. Weimann, Thermoelectric properties of GaAs-$Ga_{1-x}Al_x$As heterojunctions at high magnetic fields, Phys. Rev. B **33**, 7122 (1986).

[43] S. K. Lyo, Magnetoquantum oscillations of the phonon-drag thermoelectric power in heterojunctions, Phys. Rev. B **40**, 6458 (1989).

[44] V. C. Karavolas, G. P. Triberis, and F. M. Peeters, Electrical and thermal transport of composite fermions, Phys. Rev. B **56**, 15289 (1997).

[45] X. Zianni, P. N. Butcher, and M. J. Kearney, Semiclassical magnetothermopower of a quasi-two-dimensional electron gas, Phys. Rev. B **49**, 7520 (1994).

[46] R. Shirasaki, A. Endo, N. Hatano, and H. Nakamura, Thermomagnetic effect in the quantum Hall system, J. Electron. Mater. **41**, 1540 (2012).

[47] R. Fletcher, V. M. Pudalov, and S. Cao, Diffusion thermopower of a silicon inversion layer at low magnetic fields, Phys. Rev. B **57**, 7174 (1998).

[48] C. Possanzini, R. Fletcher, P. T. Coleridge, Y. Feng, R. L. Williams, and J. C. Maan, Diffusion Thermopower of a Two-Dimensional Hole Gas in SiGe in a Quantum Hall Insulating State, Phys. Rev. Lett. **90**, 176601 (2003).

[49] C. Possanzini, R. Fletcher, M. Tsaousidou, P. T. Coleridge, R. L. Williams, Y. Feng, and J. C. Maan, Thermopower of a p-type $Si/Si_{1-x}Ge_x$ heterostructure, Phys. Rev. B **69**, 195306 (2004).